

PFC/JA-96-9

**Survey of ICRF Heating Experiments and  
Enhanced Performance Modes in Alcator C-Mod**

Y. Takase, R.L. Boivin, F. Bombarda<sup>1</sup> P.T. Bonoli, C.L. Fiore,  
D. Garnier, J.A. Goetz, S.N. Golovato, R.S. Granetz,  
M.J. Greenwald, S.F. Horne, A.E. Hubbard, I.H. Hutchinson,  
J.H. Irby, H. Kimura<sup>2</sup>, R. Majeski<sup>3</sup>, E.S. Marmor, M. May<sup>4</sup>,  
A. Mazurenko, P. O'Shea, R. Pinsker<sup>5</sup>, M. Porkolab, J. Reardon,  
J.E. Rice, C. Rost, J. Schachter, J.A. Snipes, P. Stek,  
J.L. Terry, R.L. Watterson, B. Welch<sup>6</sup>, S.M. Wolfe

March 1996

<sup>1</sup>Associazione EURATOM-ENEA sulla Fusione, Frascati 00044 Italy.

<sup>2</sup>Japan Atomic Energy Research Institute, Naka, Ibaraki, Japan.

<sup>3</sup>Princeton Plasma Physics Laboratory, Princeton, NJ, USA.

<sup>4</sup>Dept. of Physics, The Johns Hopkins University, Baltimore, MD, USA.

<sup>5</sup>General Atomics, San Diego, CA, USA.

<sup>6</sup>Institute for Plasma Research, University of Maryland, College Park, MD, USA.

Plasma Phys. and Control. Fusion.

This work was supported by the U. S. Department of Energy Contract No. DE-AC02-78ET51013. Reproduction, translation, publication, use and disposal, in whole or in part by or for the United States government is permitted.

# Survey of ICRF heating experiments and enhanced performance modes in Alcator C-Mod

Y Takase, R L Boivin, F Bombarda†, P T Bonoli, C L Fiore, D Garnier, J A Goetz, S N Golovato, R S Granetz, M J Greenwald, S F Horne, A E Hubbard, I H Hutchinson, J H Irby, H Kimura‡, R Majeski§, E S Marmor, M May||, A Mazurenko, P O'Shea, R Pinsky¶, M Porkolab, J Reardon, J E Rice, C Rost, J Schachter, J A Snipes, P Stek, J L Terry, R L Watterson, B Welch<sup>+</sup> and S M Wolfe

MIT Plasma Fusion Center, Cambridge, MA 02139 U.S.A.

† Associazione EURATOM-ENEA sulla Fusione, Frascati 00044 Italy

‡ Japan Atomic Energy Research Institute, Naka, Ibaraki, Japan

§ Princeton University Plasma Physics Laboratory, Princeton, NJ, U.S.A.

|| Department of Physics, The John Hopkins University, Baltimore, MD, U.S.A.

¶ General Atomics, San Diego, CA, U.S.A.

<sup>+</sup> Institute for Plasma Research, University of Maryland, College Park, MD, U.S.A.

**Abstract.** Results of ICRF heating experiments in Alcator C-Mod during the November 1994 – June 1995 campaign are summarized. Efficient heating of high density ( $\bar{n}_e \lesssim 3 \times 10^{20} \text{ m}^{-3}$ ) plasmas was demonstrated with high power densities (up to  $5 \text{ MW/m}^3$  volume averaged,  $0.6 \text{ MW/m}^2$  surface averaged). These experiments were carried out with RF powers up to 3.5 MW at 80 MHz, at magnetic fields up to 8 T and plasma currents up to 1.2 MA. For on-axis hydrogen minority heating at 5.3 T, near complete absorption is achieved. Energy confinement in L-mode plasmas was found to be consistent with the ITER89-P scaling. H-mode is routinely observed when the ion  $\nabla B$

drift is directed toward the X-point. The H-mode power threshold was found to scale as low as  $P/S(\text{MW}/\text{m}^2) = 0.02\bar{n}_e B_T (10^{20} \text{m}^{-3} \text{T})$ , which is a factor of two lower than the scaling observed on other tokamaks. PEP modes with highly peaked density and ion temperature profiles and highly enhanced fusion reactivity were obtained with Li pellet injection followed by on-axis ICRF heating at both  $B_T = 5.3 \text{T}$  (H minority heating) and  $8 \text{T}$  ( $^3\text{He}$  minority heating). In H- $^3\text{He}$  plasmas at  $B_T = 6.5 \text{T}$  highly localized direct electron heating by the mode converted ion Bernstein wave was observed. Nearly complete absorption by electrons in a small volume resulted in an extremely high electron heating power density of  $P_{e0} \lesssim 30 \text{MW}/\text{m}^3$  with  $\text{FWHM} \simeq 0.2a$ .

PACS number(s): 5250, 5255, 5225F

Submitted to Plasma Phys. Control. Fusion

Date: 12 March 1996

## 1. Introduction

Alcator C-Mod ( $R = 0.67\text{ m}$ ,  $a = 0.22\text{ m}$ ,  $\kappa = 1.7$  typical) is a compact high field tokamak [1]. Initial ICRF heating results have been reported earlier [2, 3]. This paper reports the results of high power ICRF heating experiments during the operation period November 1994 – June 1995. Exploratory investigation of different heating regimes and operating modes at high ICRF heating power ( $P_{\text{RF}} \leq 3.5\text{ MW}$ ) was the main emphasis during this campaign. Further optimization and more systematic study will be carried out during the November 1995 – February 1996 campaign.

Efficient ICRF heating of high density ( $\bar{n}_e \leq 3 \times 10^{20}\text{ m}^{-3}$ ) diverted and limited plasmas was demonstrated in Alcator C-Mod, operating at very high power densities ( $P/V \lesssim 5\text{ MW/m}^3$ ,  $P/S \lesssim 0.6\text{ MW/m}^2$ , where  $P$  is the total input power,  $V$  is the plasma volume, and  $S$  is the plasma surface area). The surface power flux is in the range expected for ITER [4]. Heating consistent with the ITER89-P scaling [5] was observed in L-mode plasmas, and enhanced performance modes with improved confinement (H-mode and PEP mode) were also obtained. Direct electron heating by the mode-converted ion Bernstein wave (IBW) was also observed.

The experimental setup is described in section 2. RF power absorption and effectiveness of heating were evaluated first in L-mode plasmas, as reported in section 3. Characteristics of H-mode and PEP mode are described in sections 4 and 5, respectively. Direct electron heating is discussed in section 6, and conclusions are given in section 7.

## 2. Experimental Setup

Alcator C-Mod has operated with toroidal fields of up to 8.0 T and plasma currents of up to 1.2 MA during this campaign. Plasma facing components were all metallic. High heat flux components (the inner wall, the divertor plates, and the outboard poloidal limiters) were all armored with molybdenum tiles. Typically two hours of electron cyclotron discharge cleaning (3 kW at 2.45 GHz) in deuterium was performed prior to each run. Otherwise, no wall conditioning or coating was performed.

Two transmitters at a frequency of 80 MHz, each capable of 2 MW output, were operational. Two dipole antennas (two current straps driven out of phase) [6] were used to couple up to 3.5 MW of RF power into the plasma, which corresponds to an antenna surface power density of  $10\text{ MW/m}^2$ . The RF system operated routinely with peak RF voltages of up to 40 kV. One antenna had a TiC coated Faraday shield, while the other one had a  $\text{B}_4\text{C}$  coated Faraday shield. No significant difference was observed in the performance of the two antennas. The front surface of the Faraday shield was recessed behind the  $\text{B}_4\text{C}$  coated lateral antenna protection tiles by 5 mm. Further protection was provided by two outboard poloidal limiters at two toroidal locations, which were placed 5 mm in front of the antenna protection tiles. The radiated power fraction  $P_{\text{rad}}/P_{\text{in}}$  with ICRF heating remains the same as in ohmic plasmas. Typical value of  $P_{\text{rad}}/P_{\text{in}}$  is in the range 30 – 80%, depending on operating conditions.

The standard equilibrium was a lower single-null plasma with the inner and outer strike points on the vertical divertor plates, as shown in Figure 1. In the normal field configuration the ion  $\nabla B$  drift was directed downwards, toward the X-point. Typical parameters of the last closed flux surface were elongation of 1.6 – 1.7, lower triangularity of 0.5 – 0.55 (restricted by the placement of the strike points; the upper triangularity can be varied over a wide range), outer gap (distance between the last closed flux surface and the outboard limiter,  $d_{\text{out}}$ ) of 10 – 20 mm, and inner gap (distance between the last closed flux surface and the inner wall,  $d_{\text{in}}$ ) of 10 – 20 mm. A very small number of inner-wall limited plasmas have also been studied and yielded similar results as lower single-null diverted plasmas.

The main heating scenario employed thus far has been H minority heating in D majority plasmas at 5.3 T where single-pass absorption is predicted to be near complete (typically 80 – 100%). Single-pass absorption is estimated by running the slab geometry full-wave code FELICE [7] with a radiating boundary condition on the high field side of the resonance layer. In this paper this heating scenario will be designated by D(H), where we use the convention of indicating the minority ion species in parenthesis. Other scenarios investigated include D( $^3\text{He}$ ) at 7.9 T and mode conversion electron heating in H- $^3\text{He}$  plasmas at 6.5 T. Evidence of second harmonic H minority heating in D majority plasmas was observed at 2.6 T, during a toroidal field ramp-down, but was not studied in detail. Second harmonic  $^3\text{He}$  minority heating in D majority plasmas at 4.0 T was not successful. Large increases in molybdenum and radiated power were observed in this scenario, for which single-pass absorption is calculated to be low ( $\lesssim 10\%$ ) and the fundamental hydrogen resonance layer exists near the high-field side edge of the plasma. Boronization will be used during the 1996 campaign in an attempt to control molybdenum influx for low single-pass absorption heating schemes.

The antenna loading resistance (defined as the effective resistance at the end of a  $50\ \Omega$  transmission line) was typically 5 – 20  $\Omega$  in L-mode plasmas under normal operating conditions. Loading resistance in ELM-free H-mode plasmas was typically a factor of 2 lower than in corresponding L-mode plasmas. Vacuum loading (which represents transmission and antenna losses) was 0.25  $\Omega$ .

### 3. L-Mode

RF power absorption and effectiveness of heating were evaluated in L-mode plasmas for which energy confinement scaling is well established. D(H) heating was used because of theoretically predicted high single-pass absorption. L-mode plasmas are used as the reference for evaluating enhanced performance modes discussed in the following sections. In order to prevent transitions into H-mode at high RF powers, it was necessary to reverse the direction of the ion  $\nabla B$  drift direction (away from the X-point), operate below the H-mode low density limit ( $\bar{n}_e < 0.9 \times 10^{20} \text{ m}^{-3}$ ) [8], or operate just above the low density limit ( $\bar{n}_e \lesssim 1.1 \times 10^{20} \text{ m}^{-3}$ ) with a small outer gap

( $d_{\text{out}} \lesssim 10$  mm). A small outer gap ( $d_{\text{out}}$  as small as 5 mm) alone was not sufficient to prevent H-mode transitions.

For on-axis heating the absorption efficiency, estimated from the discontinuity of slope in the diamagnetic stored energy at RF power transitions, was typically  $\gtrsim 80\%$ . An example of a high power L-mode discharge is shown in Figure 2. Central temperatures of  $T_{e0} = 5.8$  keV (top of sawtooth) and  $T_{i0} = 4.0$  keV (sawtooth averaged) were obtained at  $\bar{n}_e = 1 \times 10^{20} \text{ m}^{-3}$  with  $P_{\text{RF}} = 3.5$  MW. Heating was observed to degrade gradually as the resonance layer was moved off-axis by reducing the toroidal field. Very little heating was observed when the resonance layer was moved out to  $r/a \geq 0.75$  ( $B_T \leq 4.1$  T).

The plasma current and input power dependences of energy confinement were roughly consistent with the ITER89-P scaling [5], as shown in Figure 3. The stored energy was evaluated using the MHD equilibrium analysis code EFIT [9], and the sum of the ohmic heating power and the injected (not absorbed) RF power was used for the input power. There was an indication of gradual degradation of confinement at higher densities [10], contrary to the  $\bar{n}_e^{0.1}$  dependence of ITER89-P L-mode scaling. The stored energy in the energetic minority ions decreases from approximately 30% at  $\bar{n}_e = 1.2 \times 10^{20} \text{ m}^{-3}$  to approximately 10% at  $\bar{n}_e = 2.2 \times 10^{20} \text{ m}^{-3}$ . There is also an indication of confinement degradation relative to the ITER89-P scaling at very low densities ( $\bar{n}_e < 1 \times 10^{20} \text{ m}^{-3}$ ), but this regime, where high  $Z_{\text{eff}}$  and  $P_{\text{rad}}/P_{\text{in}}$  are observed, was not studied in detail. The degradation at high density is observed in both ohmic and RF heated discharges, and therefore transport rather than power absorption is believed to be responsible for this behavior. In spite of the theoretical expectation that ion heating should increase at the expense of electron heating as the density is increased, less ion heating was observed compared to electron heating at high density [10], suggesting degradation of ion thermal transport as the density is increased. Further evidence of ion transport degradation at high density is provided by the minority concentration scan experiment. As shown in Figure 4 heating is found to be most effective at low H concentrations ( $n_{\text{H}}/n_e < 0.05$ ) where minority ions transfer more power to electrons. At higher H concentrations comparatively more power is transferred to ions. Degradation of heating at higher H concentrations is much more pronounced at the higher density where ion transport is believed to be degraded. More detailed transport studies will be performed during the next operation period.

#### 4. H-Mode

ICRF heated H-mode is routinely observed when the ion  $\nabla B$  drift is directed toward the X-point. Almost all high power ( $\gtrsim 2$  MW) RF heated discharges make the transition into H-mode, even with the outer gap as small as  $d_{\text{out}} = 5$  mm, although the quality of H-mode degrades as  $d_{\text{out}}$  is reduced. No special wall conditioning was required to obtain the H-mode.

An example of ICRF heated H-mode is shown in Figure 5. A transition from L-mode to ELM-free H-mode is observed, signified by a sharp drop in  $D_\alpha$  emission and a sharp density rise. In the discharge shown in Figure 5 the first ELM-free H-mode transition occurs at 0.725 s. The ELM-free H-mode usually terminates with the onset of high frequency (typically 1 – 5 kHz) ELMs while  $dW/dt$  is still a significant fraction of the total input power (the first transition to ELMy H-mode occurs at 0.775 s in the discharge shown in Figure 5). In this ELMy H-mode phase the energy confinement is only marginally better than the L-mode confinement. An H-factor (energy confinement enhancement over the ITER89-P L-mode scaling [5]) for ICRF heated ELM-free H-modes of up to 1.5 has been observed. For our parameters, ITER93 ELM-free H-mode scaling [11] predicts 1.6 – 1.8 for the H-factor, while the ELMy H-mode scaling [11] predicts 0.9 – 1.1. The highest stored energy of 130 kJ achieved in C-Mod during this campaign was obtained in an ELM-free H-mode plasma at 1.2 MA with 4.0 MW of total input power (2.4 MW RF plus 1.6 MW OH).

The H-mode power threshold (with the ion  $\nabla B$  drift directed toward the X-point) was found to scale similarly to the ASDEX-UG scaling  $P/S(\text{MW}/\text{m}^2) = 0.044 \bar{n}_e B_T$  ( $10^{20} \text{ m}^{-3} \text{ T}$ ) [12], but H-mode transitions well below this threshold (by up to a factor of 2) were often observed. Figure 6 shows L-H transitions, including those with powers well above threshold. L-H transitions are observed down to  $P/(\bar{n}_e B_T S) \simeq 0.02$ . There is a definite threshold in the edge ( $r/a = 0.85\text{--}0.95$ ) electron temperature for L-H transition [8, 13]. H-L transitions occur at the same or slightly lower edge temperatures compared to L-H transitions. We note here that the values of  $P/S$  and  $\bar{n}_e B_T$  achieved in C-Mod are an order of magnitude greater than those achieved in ASDEX-UG, DIII-D, and JET, and are comparable to or greater than what is expected for ITER. H-mode was observed up to a target density of  $\bar{n}_e = 2.6 \times 10^{20} \text{ m}^{-3}$  ( $\bar{n}_e = 3.2 \times 10^{20} \text{ m}^{-3}$  during the density decay after Li pellet injection). However, RF heated H-mode has not been observed below a low density limit of  $\bar{n}_e \simeq 0.9 \times 10^{20} \text{ m}^{-3}$ . By comparison, the low density limit for ohmic H-mode is  $\bar{n}_e \simeq 0.9 \times 10^{20} \text{ m}^{-3}$ . Only dithering was observed when the ion  $\nabla B$  drift was away from the X-point, indicating that the H-mode power threshold in this case is higher by at least a factor of 2.

The peaked density profile (i.e., lower edge density for a given line average density, allowing higher edge temperature) after Li pellet injection seems to be beneficial for accessing the H-mode. The local edge ( $r/a = 0.85$ ) electron temperature at L-H and H-L transitions for plasmas with Li pellet injection do not differ significantly from those without pellet injection. A low neutral pressure at the outboard midplane of the main chamber is also believed to be beneficial in obtaining a high-quality H-mode [14]. For the next operation period, a modification was made to the outer divertor to prevent leakage of neutrals to the main chamber, and boronization will be used in an attempt to reduce the midplane neutral density and to reduce the molybdenum impurity influx.

## 5. PEP Mode

Confinement improvement using pellet injection (P-mode) was first discovered in Alcator C [15,16]. Particle transport and ion thermal transport were reduced to near neoclassical values. In JET, central ICRF heating was applied in combination with pellet injection to produce the pellet enhanced performance (PEP) mode [17, 18]. The key ingredients are core particle fueling and core ion heating resulting in highly peaked density and ion temperature profiles, greatly reduced transport in the plasma core (transport barrier formation), and a greatly enhanced fusion neutron rate. Shear reversal in the plasma core region was also observed. The PEP mode appears to have some common features with the recently discovered enhanced performance modes such as the NCS mode in DIII-D [19,20], the ERS mode in TFTR [21], and the high  $\beta_p$  mode [22] and the reversed shear mode in JT-60U [23].

In Alcator C-Mod, PEP mode was obtained by combining Li pellet ( $1.2 \times 10^{20}$  electrons) injection and on-axis ICRF minority heating. The PEP mode is observed over a wide range of target densities,  $\bar{n}_e = (1.0 - 2.5) \times 10^{20} \text{ m}^{-3}$ , but only when the pellet penetrates to the plasma core. The central  $Z_{\text{eff}}$  increases transiently after pellet injection, but decays over a time scale of approximately 20 ms, indicating replacement of Li ions by D ions. Sawtooth suppression is almost always observed after pellet injection, but PEP mode without sawtooth suppression has also been observed. The current density profile (and the  $q$  profile) evolution calculated by TRANSP shows increase of the central  $q$  above 1 from increased resistivity (caused by transiently increased  $Z_{\text{eff}}$  and decreased  $T_e$ ), followed by shear reversal in the plasma core driven by off-axis bootstrap current as the pressure gradient builds up. Shear reversal in the core region was experimentally observed in 5.3 T PEP modes using the Li pellet ablation diagnostic [24]. The enhancement of the fusion neutron rate is typically an order of magnitude over similar L-mode discharges.

In the 7.9 T, 1.0 MA discharge shown in Figure 7 a fusion neutron rate of  $R_{\text{DD}} = 0.9 \times 10^{14} \text{ s}^{-1}$  was obtained with  $P_{\text{RF}} = 2.5 \text{ MW}$ . In this D( $^3\text{He}$ ) heating scenario the incremental neutron production is thermonuclear. Unlike in the D(H) case, enhancement due to superthermal deuterons created by second harmonic absorption can be ruled out. Power deposition during PEP mode is highly peaked because of wave focusing. Energetic minority ion distribution is not formed because of high central density, and most of the power is deposited on ions in the plasma core as shown in Figure 8. In L-mode most of the power is deposited on electrons in the plasma core, with a broader deposition on ions. The density and temperature profiles at the time of maximum pressure (0.82 s) are shown in Figure 9, compared with ohmic and L-mode profiles. The density profile shape during the PEP mode used in the analysis (shown by the dashed line) is based on later PEP mode discharges when an additional Thomson scattering data point at  $r/a \simeq 0.4$  was available. The near central ( $r/a = 0.1$ ) values of density and temperatures were  $n_e = 8.2 \times 10^{20} \text{ m}^{-3}$ ,  $T_i = 3.4 \text{ keV}$ , and  $T_e = 2.8 \text{ keV}$ , resulting in a very high plasma pressure of 0.8 MPa (8



atmospheres). The peaking of the electron temperature profile was less pronounced than those of density and ion temperature profiles. The highly peaked density and ion temperature profiles imply improved particle and ion thermal diffusivities in the plasma core ( $r/a \lesssim 0.3$ ). The results of transport analysis using TRANSP indicate reduction of core thermal diffusivities, as shown in Figure 10.

H-mode transitions are often observed during the PEP mode. In the example shown in Figure 7 a transition into ELMy H-mode occurred at 0.828 s and a transition into ELM-free H-mode occurred at 0.845 s, but the neutron rate starts to decline after 0.830 s, before the ELM-free H-mode transition. Simultaneous PEP and H-modes (i.e., the peak of the neutron rate during the ELM-free H-mode phase) have also been observed. The cause of PEP mode termination is not well understood. It is sometimes, but not always, accompanied by enhanced MHD activity. PEP mode termination appears to be related to the loss of the peaked density profile. The neutron rate starts to decline when the density peak-to-volume-average ratio  $n_{e0}/\langle n_e \rangle$  falls below a critical level of approximately 3. Shear reversal is maintained for at least 10 ms after the neutron rate starts to decline.

## 6. Mode Conversion Electron Heating

Highly localized direct electron heating using the mode converted ion Bernstein wave (IBW) [25, 26, 27] was observed in H-<sup>3</sup>He plasmas at 6.5 T. H-<sup>3</sup>He plasmas are analogous to D-T plasmas, because  $\Omega_H/\Omega_{^3\text{He}} = \Omega_D/\Omega_T$ . At this field, the H resonance is at  $R = 0.83$  m and the <sup>3</sup>He resonance is at  $R = 0.55$  m, both more than half way out radially from the plasma center. Mode conversion to IBW occurs near the ion hybrid layer, which shifts toward the high field side as the <sup>3</sup>He concentration is decreased or the toroidal field is reduced. The ion Bernstein wave is strongly damped near the mode conversion layer [28]. Effective central electron heating was observed with  $n_{^3\text{He}}/n_e \simeq 0.25$  when mode conversion occurs near the plasma center, as depicted in Figure 11. Highly peaked electron heating profile is predicted by the slab geometry full-wave code FELICE [7]. Note that there is a possibility of weaker off-axis absorption of the fast wave by electrons and hydrogen ions. In toroidal geometry, the absorbed power density near the plasma axis is amplified due to wave focusing.

The <sup>3</sup>He concentration was estimated from the density rise due to <sup>3</sup>He gas puffing, spectroscopic measurements of the HeII Ly $\alpha$  line, and  $Z_{\text{eff}}$ . The main diagnostic used to study electron heating was a 9-channel ECE polychromator. A central electron temperature increase from 2.3 keV to 5.1 keV was observed with  $P_{\text{RF}} = 1.3$  MW, as shown in Figure 12. The neighboring polychromator channel (only 0.03 m away) shows much less temperature rise, indicating extremely localized heating. This feature is particularly useful for perturbative transport studies, which we will pursue in the future. With D(H) minority heating under similar conditions, approximately 3 MW of RF power was required to achieve the same central electron temperature. However,

with this scheme of direct electron heating much less ion heating was observed compared to D(H) minority heating, which heats both electrons and ions.

The electron temperature shows a clear break in slope when the RF power is switched off [29], indicating direct electron heating. The electron heating power density can be evaluated from this discontinuity in slope. When the power deposition is inside the sawtooth inversion radius the RF power deposition profile can also be determined from the difference in the sawtooth reheat rate between RF heated and ohmic phases. When both measurements are available, the two methods yield the same result. The RF power deposition profile for on-axis heating is shown in Figure 13. For on-axis heating a central electron heating power density of up to  $30 \text{ MW/m}^3$  was obtained with  $P_{\text{RF}} = 1.2 \text{ MW}$ , over an order of magnitude larger than the ohmic value with  $P_{\text{OH}} = 1.1 \text{ MW}$ . The heating profile was highly peaked with a FWHM of  $0.05 \text{ m}$ , compared to a typical FWHM of  $0.13 \text{ m}$  for H minority heating. The volume integral of the electron heating profile was typically in the range  $50 - 100\%$  of the injected RF power. The power deposition zone moves off-axis at both lower and higher  $^3\text{He}$  concentrations, consistent with the shift of the mode conversion layer. Similarly, the power deposition zone moves off-axis as the field is lowered to  $6.0 \text{ T}$  [30]. A slightly hollow electron temperature profile was observed for off-axis heating. An obvious application of this scheme is off-axis current drive to produce and maintain the reversed shear current density profile.

## 7. Conclusions

Efficient high power density ICRF heating of high density ( $\bar{n}_e \lesssim 3 \times 10^{20} \text{ m}^{-3}$ ) plasmas was demonstrated in Alcator C-Mod at ITER relevant power densities ( $P/S \lesssim 0.6 \text{ MW/m}^2$ ). For on-axis D(H) heating near complete absorption was achieved. Central temperatures of  $T_{e0} = 5.8 \text{ keV}$  (top of sawtooth) and  $T_{i0} = 4.0 \text{ keV}$  (sawtooth averaged) were obtained in an L-mode plasma at  $\bar{n}_e = 1 \times 10^{20} \text{ m}^{-3}$  with  $3.5 \text{ MW}$  of RF power. The energy confinement in L-mode plasmas was found to be consistent with the ITER89-P scaling. H-mode is routinely observed when the ion  $\nabla B$  drift is directed toward the X-point. The H-mode power threshold was found to scale as low as  $P/S (\text{MW/m}^2) = 0.02 \bar{n}_e B_T (10^{20} \text{ m}^{-3} \text{ T})$ , which is a factor of two lower than the scaling observed on other tokamaks. H-factors of up to 1.5 have been observed in ELM-free H-mode plasmas, comparable to 1.6–1.8 predicted by the ITER94 ELM-free H-mode scaling. The highest stored energy of  $130 \text{ kJ}$  was achieved in an ELM-free H-mode plasma, while the highest fusion reactivity of  $0.9 \times 10^{14} \text{ s}^{-1}$  was obtained in a PEP mode plasma with Li pellet injection and on-axis ICRF heating. These discharges have highly peaked density and ion temperature profiles, and enhanced fusion reactivity (typically an order of magnitude above similar L-mode discharges). Transport analysis of PEP mode plasmas indicate a large reduction of thermal transport in the plasma core. Further optimization of both H-mode and PEP mode will be pursued during the next operation period. At  $B_T = 6.5 \text{ T}$  highly localized direct electron heating

by the mode converted IBW was observed in H-<sup>3</sup>He plasmas. The near term (1996 – 1997) plans call for the addition of 4 MW of tunable (40 – 80 MHz) power and a FWCD/MCCD (fast wave current drive and mode conversion current drive) antenna in collaboration with PPPL.

## Acknowledgments

This work was supported by the U.S. Department of Energy Contract No. DE-AC02-78ET51013.

## References

- [1] Hutchinson I H et al 1994 *Phys. Plasmas* **1** 1511
- [2] Takase Y et al 1995 *Fusion Engineering and Design* **26** 89
- [3] Porkolab M et al 1995 *Proc. 15th Int. Conf. Plasma Physics and Contr. Nucl. Fusion Res., Seville 1994*, vol 1 (Vienna: IAEA) p. 123
- [4] ITER-JCT and Home Teams (presented by Janeschitz G) 1995 *Plasma Phys. Control. Fusion* **37** A19
- [5] Yushmanov P G et al 1990 *Nucl. Fusion* **30** 1999
- [6] Takase Y et al 1992 *Proc. 14th IEEE/NPSS Symp. Fusion Engineering, San Diego* (Piscataway, New Jersey: IEEE) p. 118
- [7] Brambilla M 1988 *Nucl. Fusion* **28** 549
- [8] Snipes J A et al 1996 to be published in *Plasma Phys. Control. Fusion*
- [9] Lao L L et al 1985 *Nucl. Fusion* **25** 1611
- [10] Golovato S N et al 1995 *Proc. 11th Top. Conf. on Radio Frequency Power in Plasmas, Palm Springs* (New York: AIP) p. 23
- [11] Thomsen K et al 1994 *Nucl. Fusion* **34** 131
- [12] Ryter F et al 1993 *Proc. 20th EPS Conf. on Contr. Fusion and Plasma Physics, Lisboa*, vol 17C (Geneva: EPS) p. I-23
- [13] Hubbard A et al 1995 *Bull. Am. Phys. Soc.* **40** 1698
- [14] Snipes J et al 1996 *Phys. Plasmas* (to be published).
- [15] Greenwald M et al 1984 *Phys. Rev. Lett.* **53** 352
- [16] Wolfe S M et al 1986 *Nucl. Fusion* **26** 319
- [17] JET Team (presented by Schmidt G L) 1989 *Proc. 12th Int. Conf. Plasma Physics and Contr. Nucl. Fusion Res., Nice 1988*, vol 1 (Vienna: IAEA) p. 215
- [18] Tubbing B, et al 1991 *Nucl. Fusion* **31**, 839
- [19] Lazarus E A et al 1992 *Phys. Fluids B* **4** 3644
- [20] Strait E J et al 1995 *Phys. Rev. Lett.* **75** 4421
- [21] Levington F M et al 1995 *Phys. Rev. Lett.* **75** 4417
- [22] Ishida S et al 1993 *Proc. 14th Int. Conf. Plasma Phys. Contr. Nucl. Fusion Res., Würzburg 1992*, vol 1 (Vienna: IAEA) p. 219
- [23] Kimura H et al 1996 *Phys. Plasmas* to be published
- [24] Marmar et al 1995 *Bull. Am. Phys. Soc.* **40** 1701
- [25] Majeski R et al 1994 *Phys. Rev. Lett.* **73** 2204
- [26] Majeski R et al 1996 *Phys. Rev. Lett.* **76** 764
- [27] Saoutic B et al 1995 *Proc. 11th Top. Conf. on Radio Frequency Power in Plasmas, Palm Springs* (New York: AIP) p. 71
- [28] Ram A K and Bers A 1991 *Phys. Fluids B* **3** 1059
- [29] Takase Y et al 1995 *Proc. 11th Top. Conf. on Radio Frequency Power in Plasmas, Palm Springs* (New York: AIP) p. 75
- [30] Takase Y et al 1995 *Proc. 22nd EPS Conf. on Control. Fusion and Plasma Physics, Bournemouth*, vol 19C (Geneva: EPS) p. II-341

## Figure captions

**Figure 1.** A typical lower single-null equilibrium.  $B_T = 5.4$  T,  $I_p = 1.0$  MA,  $R = 0.67$  m,  $a = 0.21$  m,  $\kappa_x = 1.7$ ,  $\delta_x^u = 0.36$ ,  $\delta_x^l = 0.55$ ,  $\beta_p = 0.32$ ,  $\ell_i = 1.20$ . The structure on the outboard side is the limiter. The front surface of the antenna Faraday shield is located 10 mm farther out.

**Figure 2.** An example of a high power L-mode discharge.  $B_T = 5.3$  T,  $I_p = 0.82$  MA,  $P_{RF} = 3.5$  MW.

**Figure 3.** L-mode confinement data. The MHD stored energy is plotted as a function of the total input power for four different currents. Solid lines represent the ITER89-P scaling.

**Figure 4.** Dependence of the MHD stored energy on the minority ion concentration in L-mode plasmas at two different densities,  $\bar{n}_e = 1.2 \times 10^{20} \text{ m}^{-3}$  and  $\bar{n}_e = 1.8 \times 10^{20} \text{ m}^{-3}$ .

**Figure 5.** An example of ICRF heated H-mode. The MHD energy confinement time is compared with L-mode and H-mode scalings. Alternating ELM-free and ELMy H-modes are observed.

**Figure 6.** H-mode power threshold. The line labeled  $P/S = 0.044 nB$  indicates the ASDEX-UG H-mode threshold scaling [12]. Li pellet fuelled plasmas (indicated by open symbols) generally exhibit lower power thresholds. The two data points at highest values of  $\bar{n}_e B_T$  were obtained at 7.9 T.

**Figure 7.** D(<sup>3</sup>He) PEP mode at  $B_T = 7.9$  T and  $I_p = 1.0$  MA. A Li pellet was injected at 0.761 s, and the RF power was turned on at 0.776 s. The square symbols indicate Thomson scattering times ( $n_{e0}$ ) and EFIT analysis times ( $W_{MHD}$ ).

**Figure 8.** RF heating power profiles calculated by TRANSP for PEP mode and L-mode. The ohmic heating power profile is also shown for comparison.

**Figure 9.** Density and temperature profiles during PEP mode compared with ohmic and L-mode profiles.

**Figure 10.** Thermal diffusivities at  $r/a = 0.2$  determined from TRANSP analysis. The transient around the pellet injection time (0.75–0.79 s) is not physical.

**Figure 11.** Mode conversion geometry for  $B_T = 6.5$  T,  $n_{sHe}/n_e \simeq 0.25$ . Ion resonances are located off-axis whereas the mode conversion layer is located near the plasma axis. Slab geometry full-wave code (FELICE) predicts highly localized electron Landau damping of the mode-converted IBW. In toroidal geometry, the absorbed power density near the plasma axis is amplified due to wave focusing.

**Figure 12.** An example of on-axis mode conversion electron heating at  $B_T = 6.5$  T and  $I_p = 0.82$  MA. The magnetic axis is located at  $R = 0.68$  m. Note the difference in response between  $R = 0.67$  m and  $R = 0.64$  m.

**Figure 13.** Power deposition profile for on-axis mode conversion electron heating determined from the discontinuity of the electron heating rate at RF turn-off.  $B_T = 6.4$  T,  $I_p = 0.80$  MA,  $P_{RF} = 1.2$  MW.

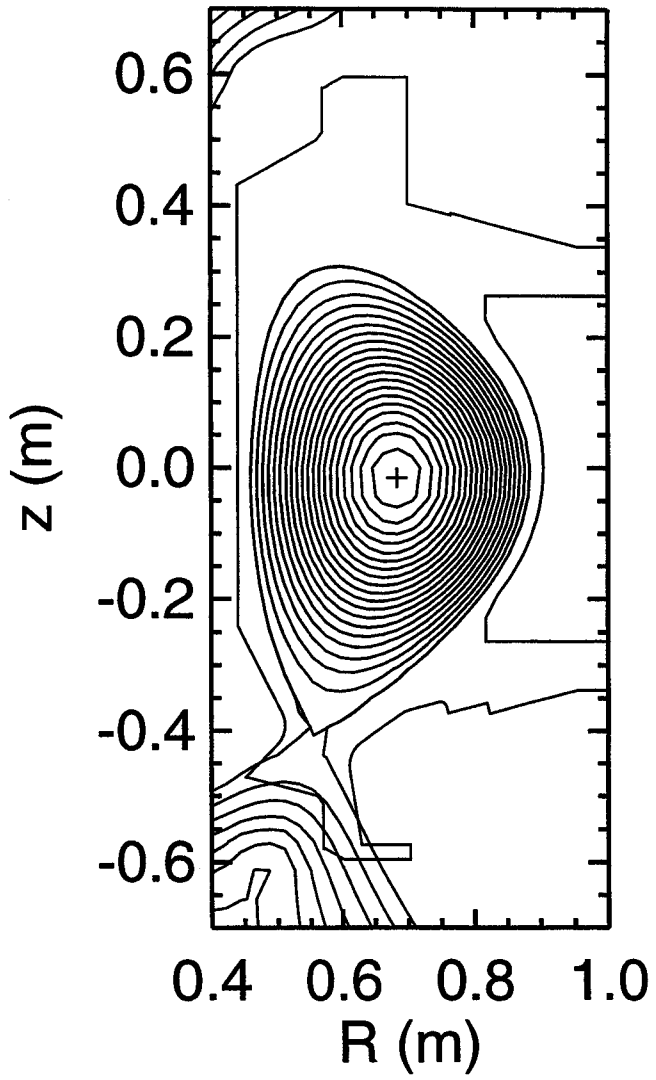


Figure 1

C-Mod Shot 950118033

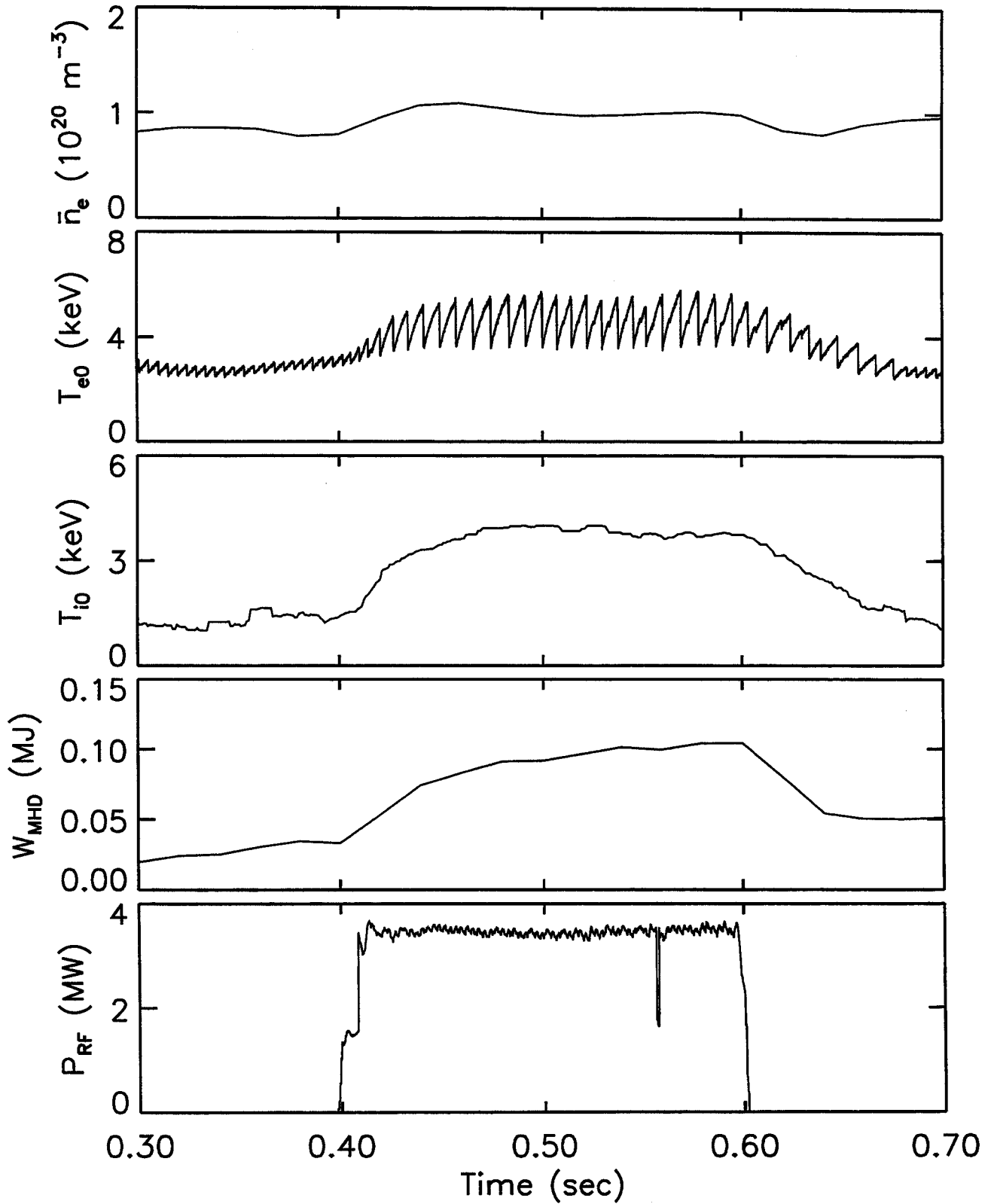


Figure 2

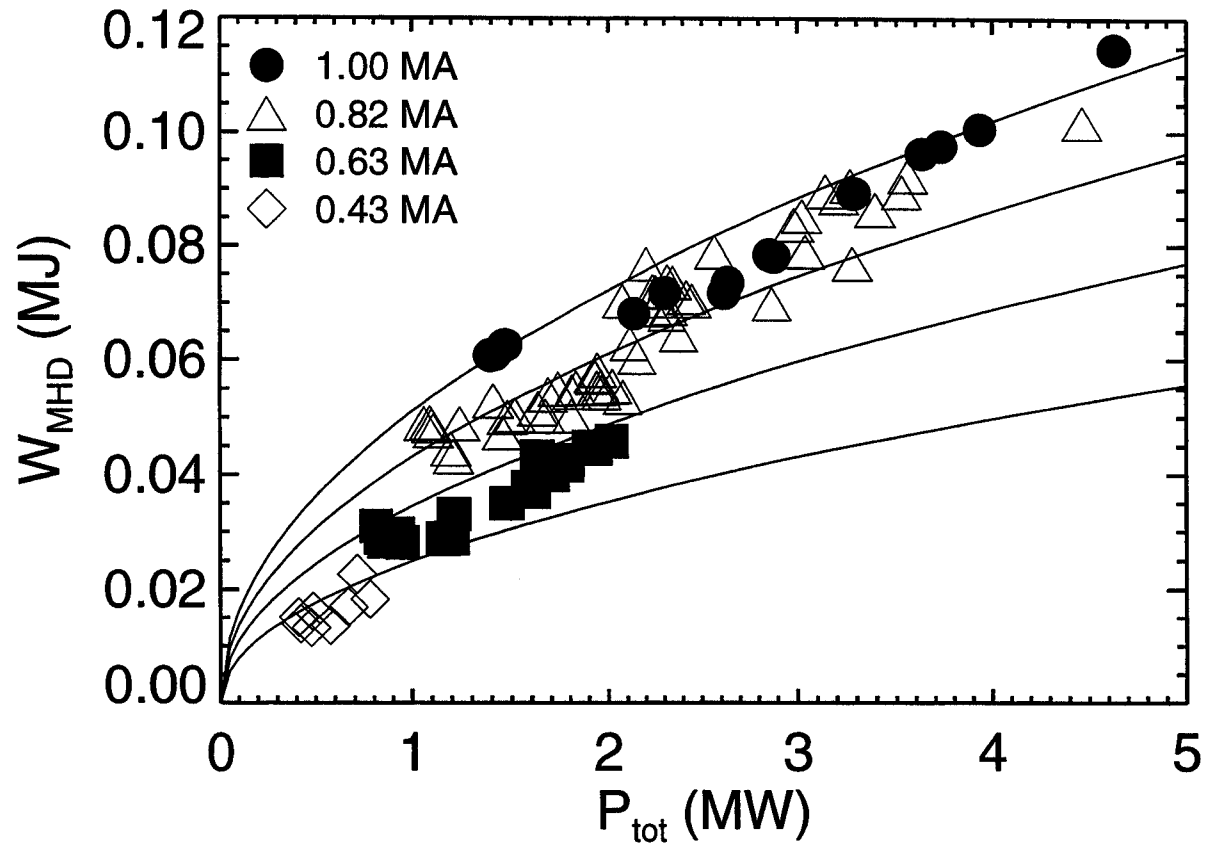


Figure 3

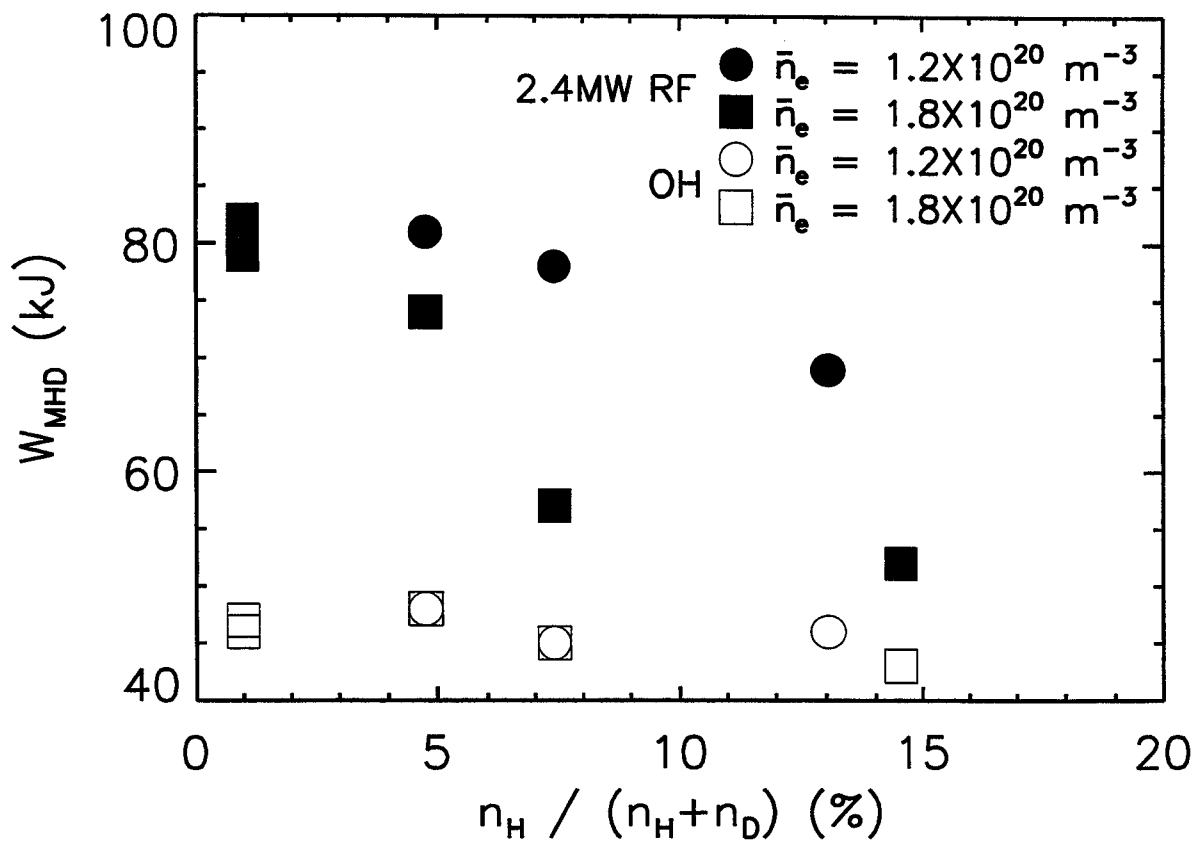


Figure 4



C-Mod Shot 950331038

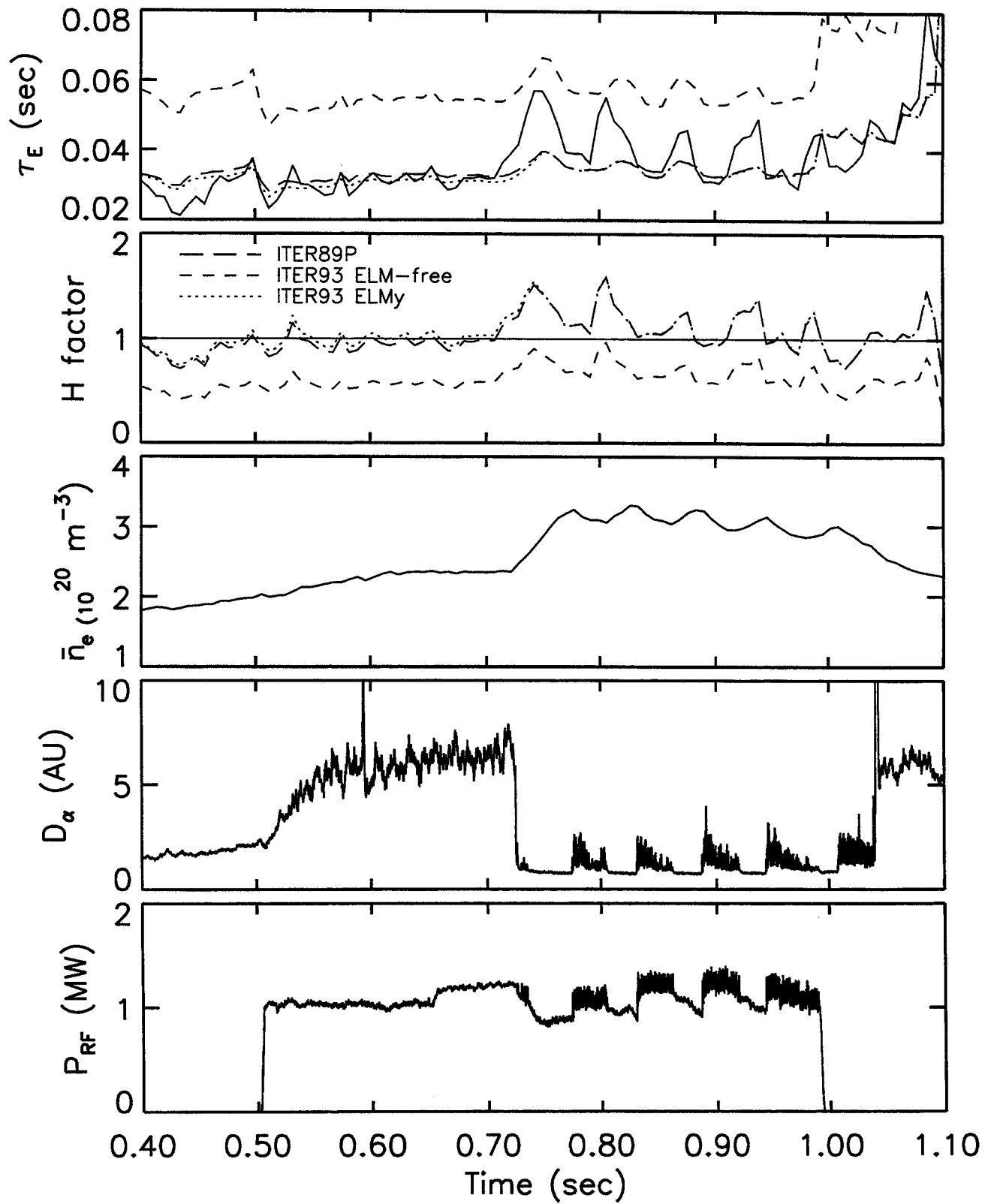


Figure 5

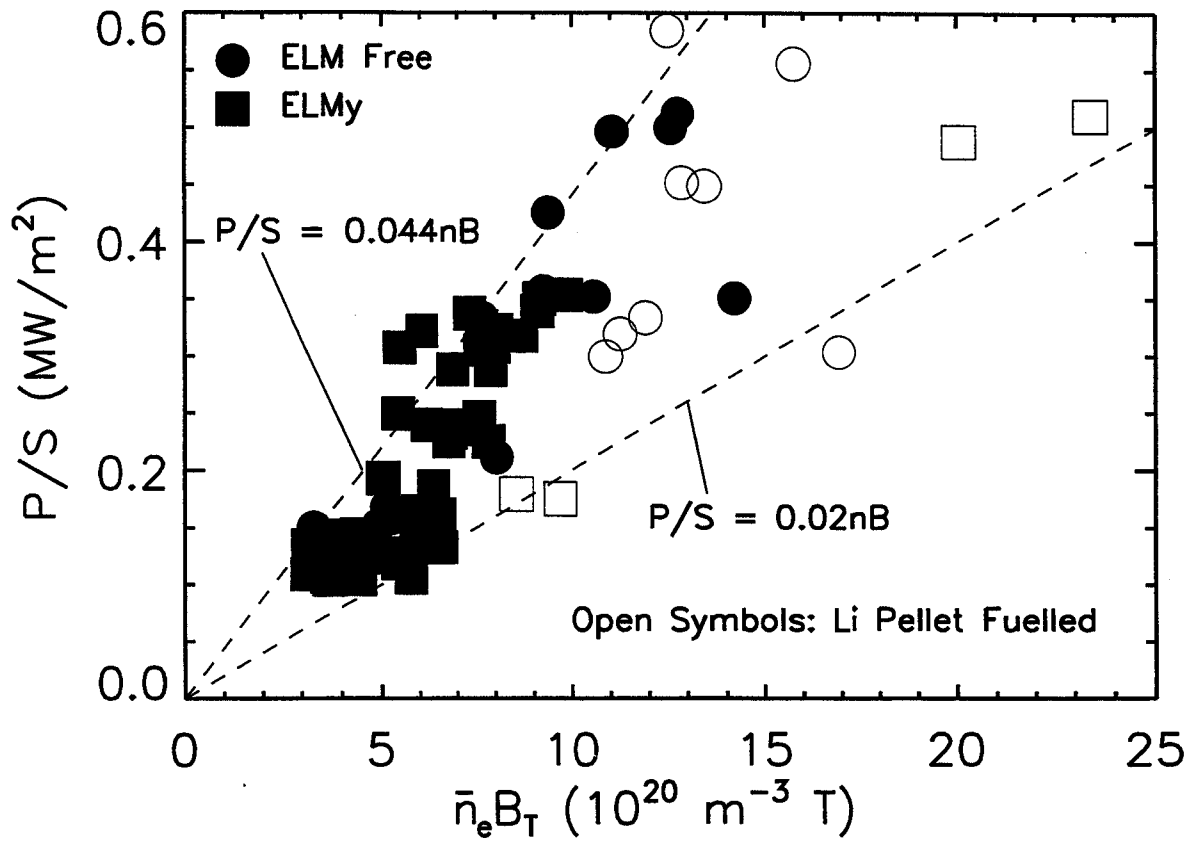


Figure 6

C-Mod Shot 950609013

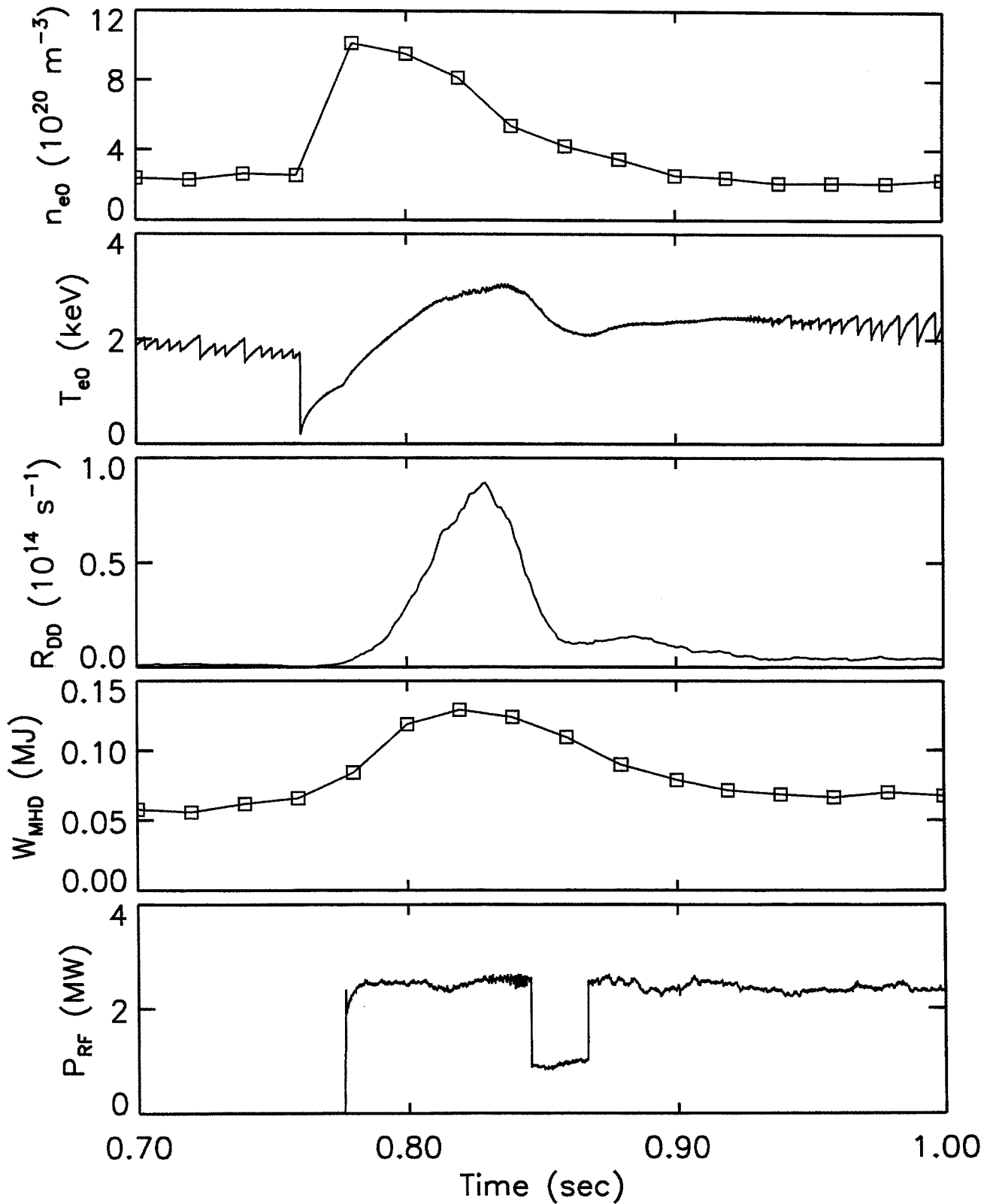
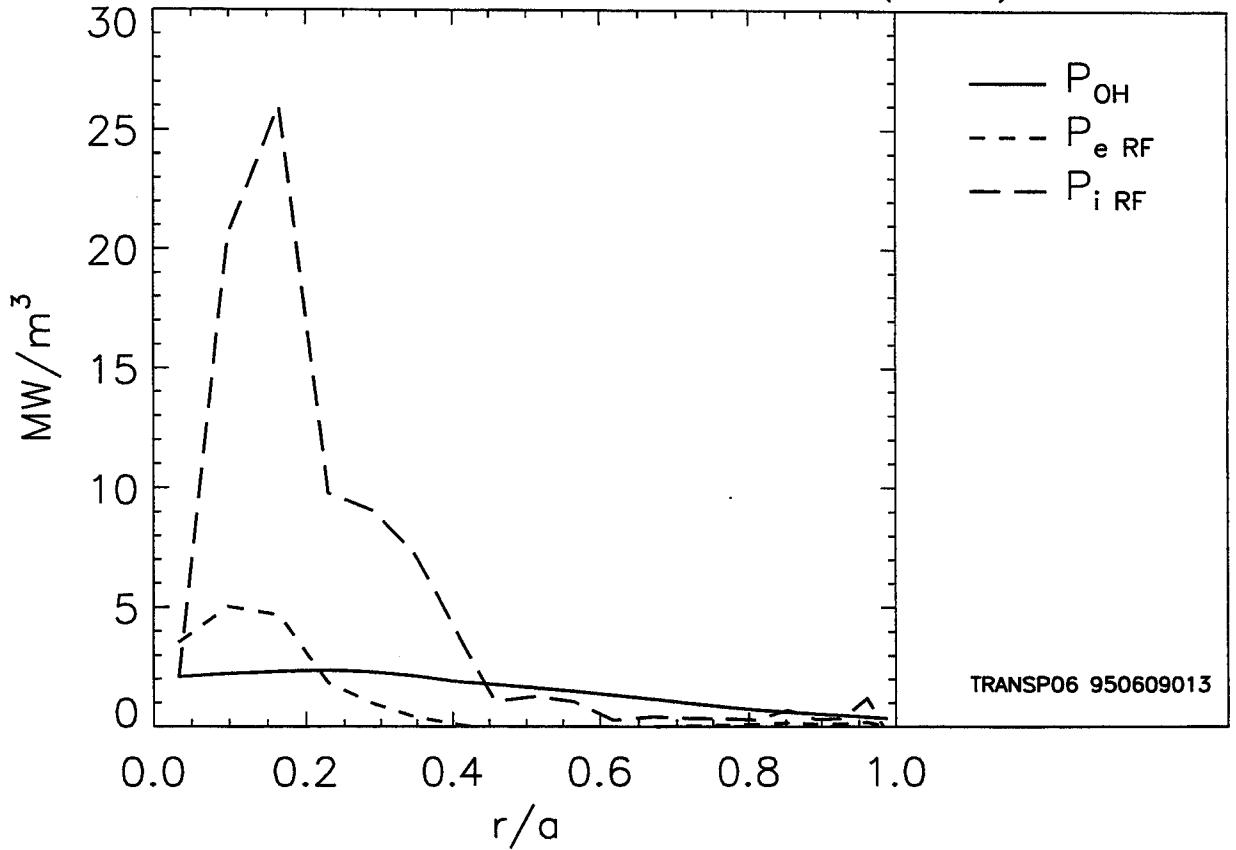


Figure 7  
18

### Heating Powers at $t = 0.820$ s (PEP)



### Heating Powers at $t = 0.960$ s (L)

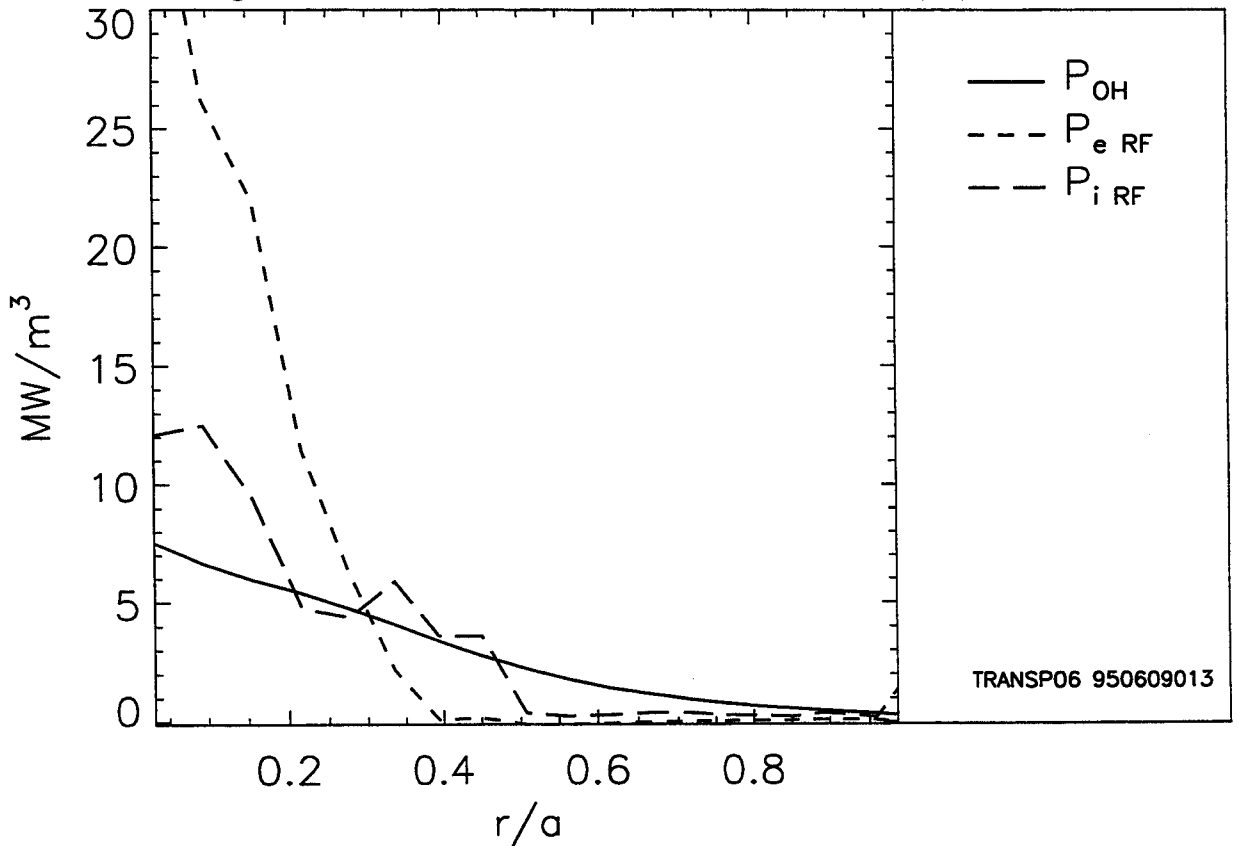


Figure 8  
19

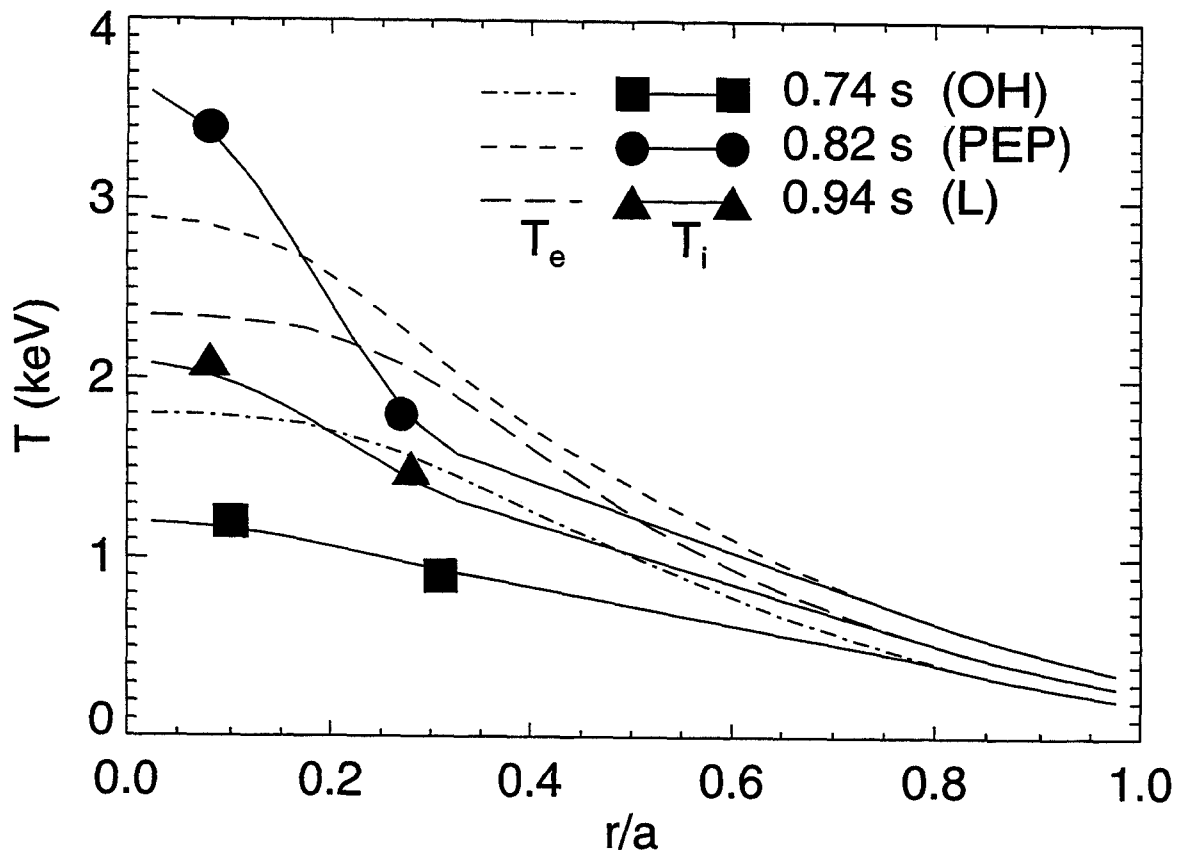
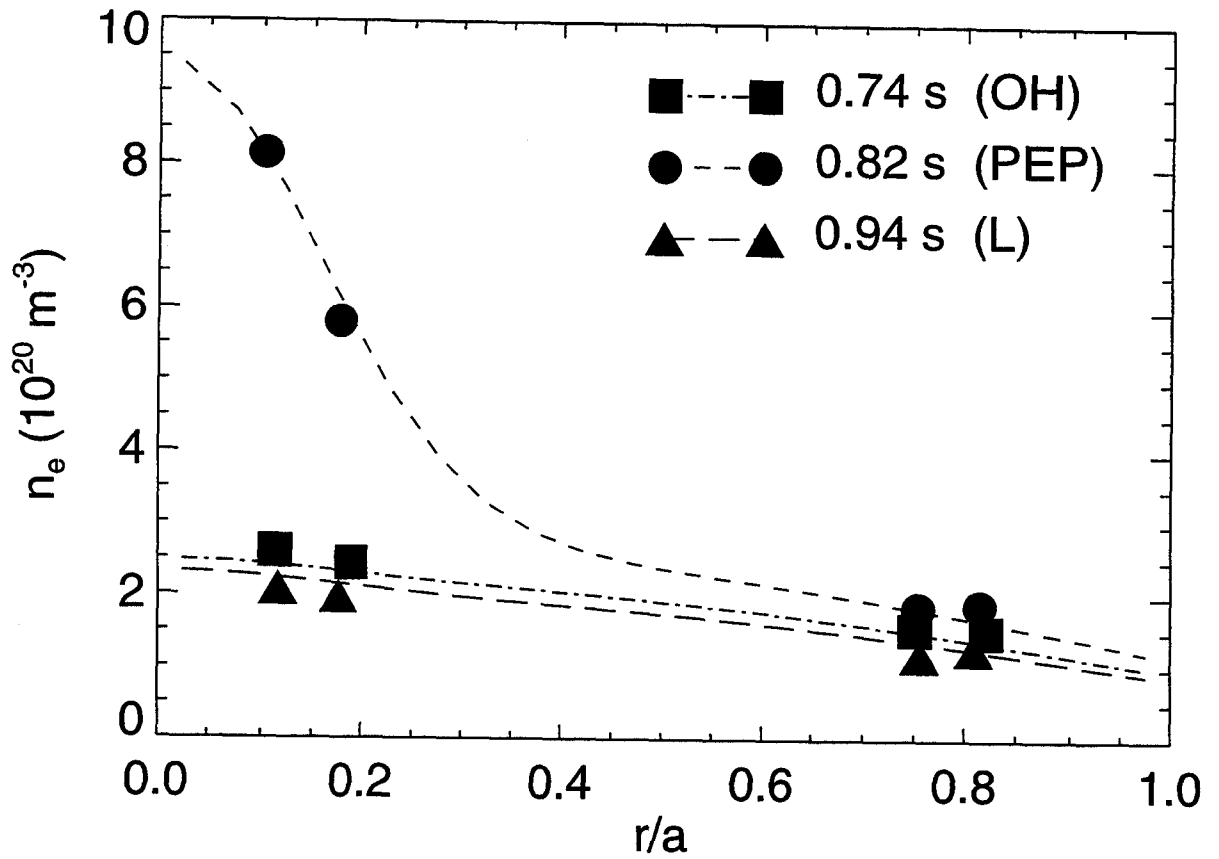


Figure 9

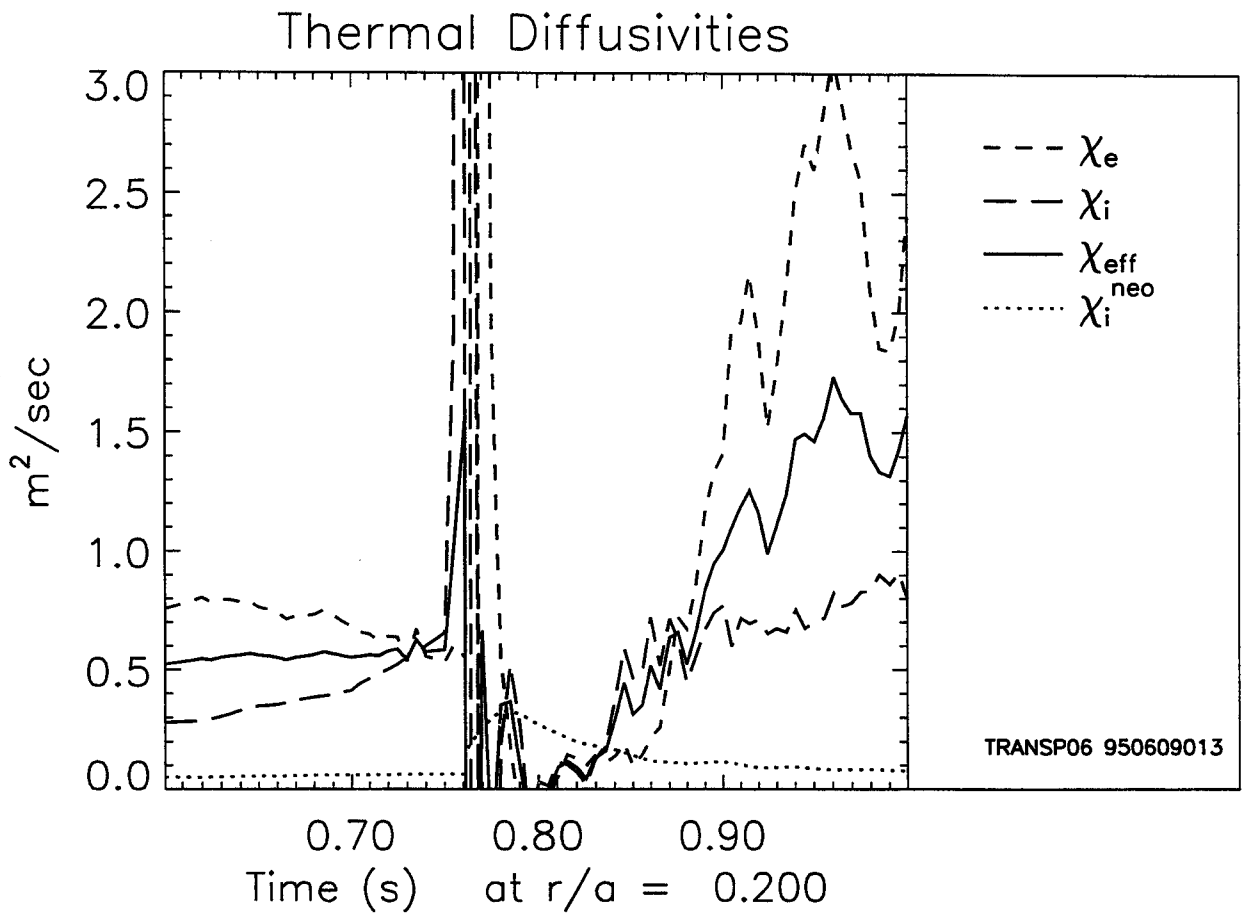


Figure 10

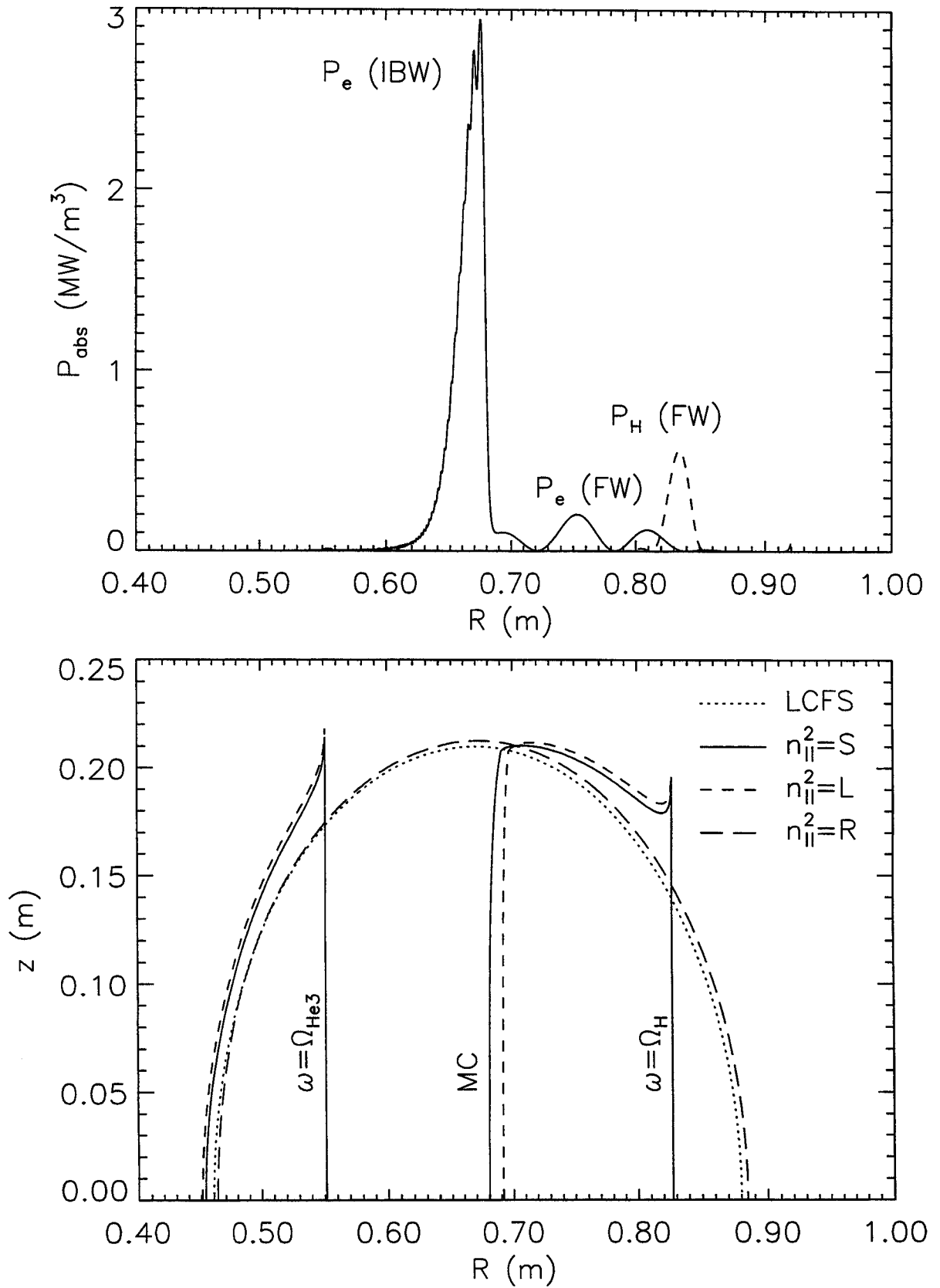


Figure 11

C-Mod Shot 950511016

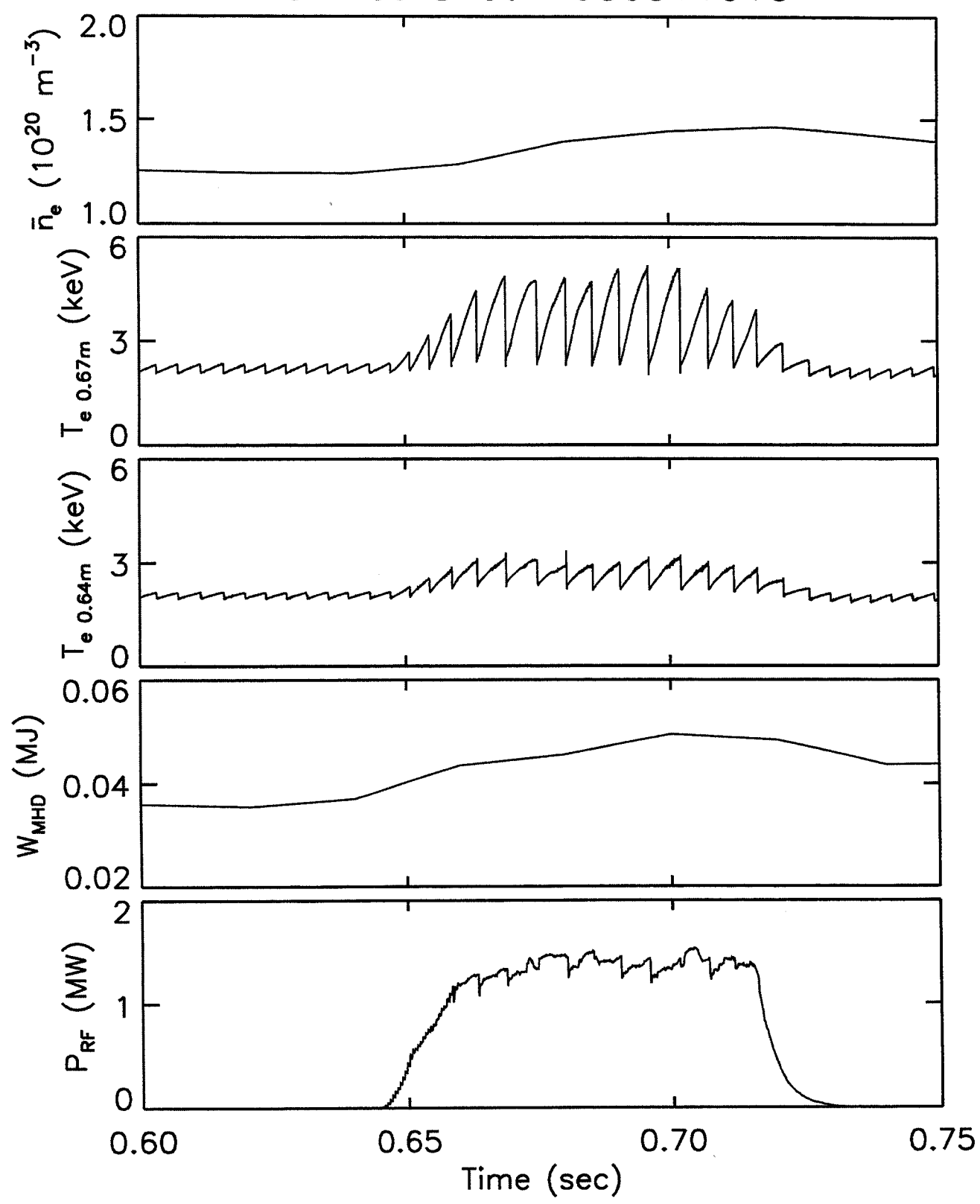


Figure 12



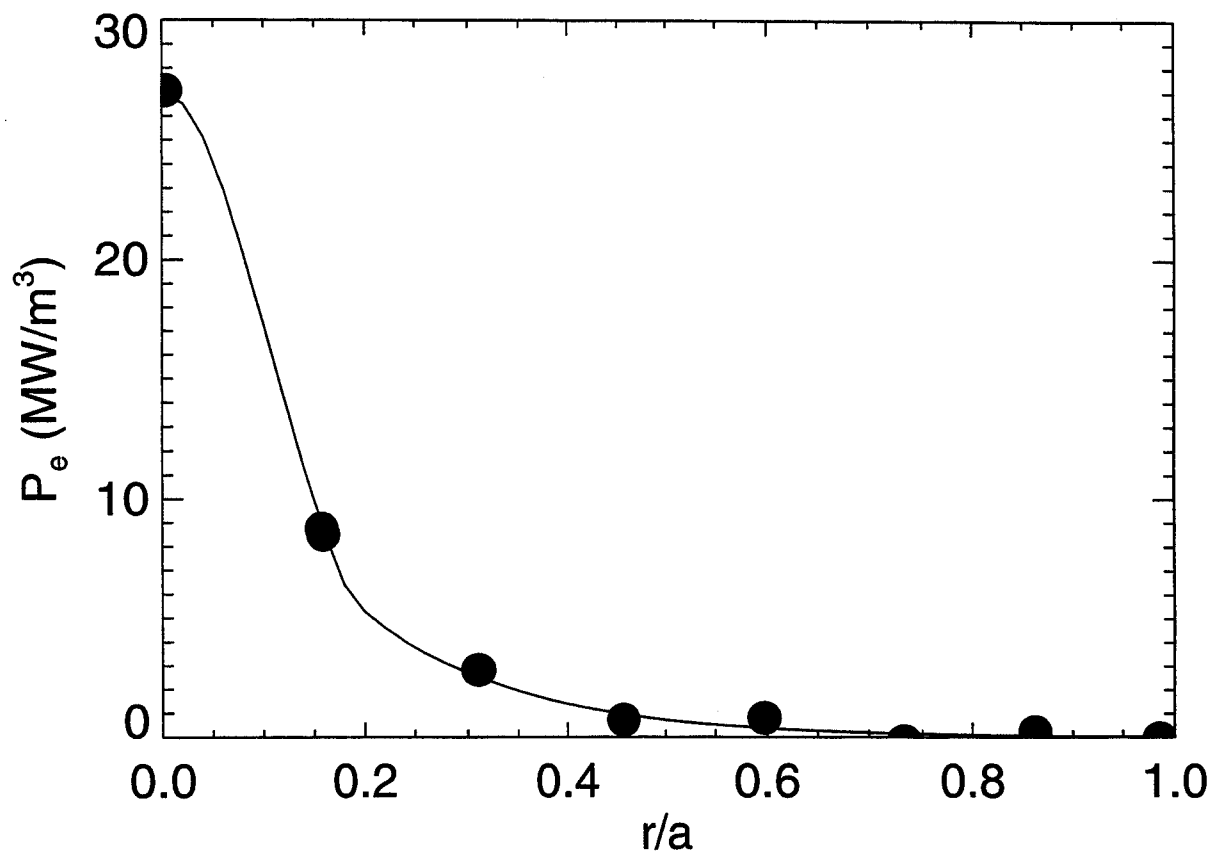


Figure 13